ACS NANO

www.acsnano.org

ARTICLE

Mechanically Stiff Nanocomposite Hydrogels at Ultralow Nanoparticle Content

Manish K. Jaiswal,[†] Janet R. Xavier,[†] James K. Carrow,[†] Prachi Desai,[†] Daniel Alge,[†,‡] and Akhilesh K. Gaharwar*[,†,‡,§]

[†]Department of Biomedical Engineering, Texas A&M University, College Station, Texas 77843, United States
[‡]Department of Materials Science and Engineering, Texas A&M University, College Station, Texas 77843, United States
[§]Center for Remote Health Technologies and Systems, Texas A&M University, College Station, Texas 77843, United States

Supporting Information

ABSTRACT: **Although hydrogels are able to mimic native tissue microenvironments, their utility for biomedical applications is severely hampered due to limited mechanical stiffness and low toughness. Despite recent progress in designing stiff and tough hydrogels, it is still challenging to achieve a cell-friendly, high modulus construct. Here, we report a highly efficient method to reinforce collagen-based hydrogels using extremely low concentrations of a nanoparticulate-reinforcing agent that acts as a cross-link epicenter. Extraordinarily, the addition of these nanoparticles at a 10 000-fold lower concentration relative to polymer resulted in a more than 10-fold increase in mechanical stiffness and a 20-fold increase in toughness. We attribute the high stiffness of the nanocomposite network to the chemical functionality of the nanoparticles, which enabled the cross-linking of multiple polymeric chains to the nanoparticle surface. The mechanical stiffness of the nanoengineered hydrogel can be tailored between 0.2 and 200 kPa simply by manipulating the size of the nanoparticles (4, 8, and 12 nm), as well as the concentrations of the nanoparticles and polymer. Moreover, cells can be easily encapsulated within the nanoparticulate-reinforced hydrogel network, showing high viability. In addition, encapsulated cells were able to sense and respond to matrix stiffness. Overall, these results demonstrate a facile approach to modulate the mechanical stiffness of collagen-based hydrogels and may have broad utility for various biomedical applications, including use as tissue-engineered scaffolds and cell/protein delivery vehicles.**

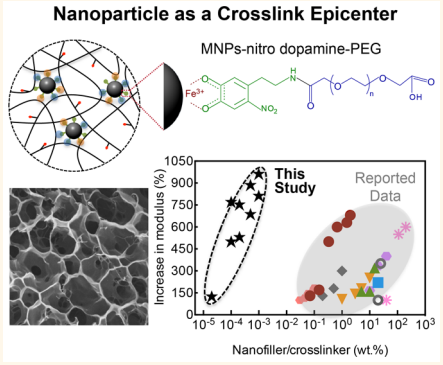

KEYWORDS: *nanocomposites, hydrogels, mechanical stiffness, nanoparticles, tissue engineering*

Hydrogels are highly hydrated three-dimensional polymeric networks that can mimic the native tissue microenvironment;[1] however, their utility for biomedical applications is severely hampered due to limited mechanical stiffness and low toughness.[2−6] Despite recent progress in designing stiff and tough hydrogels, it is still challenging to achieve a cell-friendly, high modulus construct.[7−10] A range of chemical and physical mechanisms have been proposed to enhance the mechanical stiffness of hydrogel networks including double-network hydrogels,[11] supramolecular or topological hydrogels,[12] microsphere-cross-linked hydrogels,[13] nanoclay-cross-linked hydrogels,[14−16] and hybrid physically/chemically cross-linked hydrogels.[17] Nevertheless, most of these modifications either require the hydrogels to be formed under conditions that are not suitable for cell encapsulation or need a high concentration of reinforcing agent. Thus, there has been unprecedented interest in developing advanced strategies to design and develop mechanically stiff hydrogels for engineered tissue structures.

Recently, collagen-based hydrogels have been extensively investigated for cell and tissue engineering applications owing to their ability to encapsulate cells, nonimmunogenic properties, ability to mimic the native extracellular matrix (ECM) and biodegradable characteristics.[18] There have been several efforts to fabricate mechanically robust collagen-based hydrogels by covalent cross-linking, interpenetrating networks, and nanocomposite structures.[19−22] However, these techniques cause significant decreases in porosity and hydration degree, which are important drawbacks. Recently, one-dimensional nanomaterials such as carbon nanotubes (CNTs)[20,21] and two-dimensional nanomaterials such as graphene, graphene oxide (GO),[19] and synthetic silicate nanoparticles[22] have been incorporated into collagen-based (gelatin) hydrogels to enhance the mechanical stiffness of these materials.[20,21] These nanoparticles physically and/or chemically interact with polymer and enhance the

Received: June 26, 2015
Accepted: December 15, 2015
Published: December 15, 2015

DOI: 10.1021/acsnano.5b03918
ACS Nano 2016, 10, 246−256

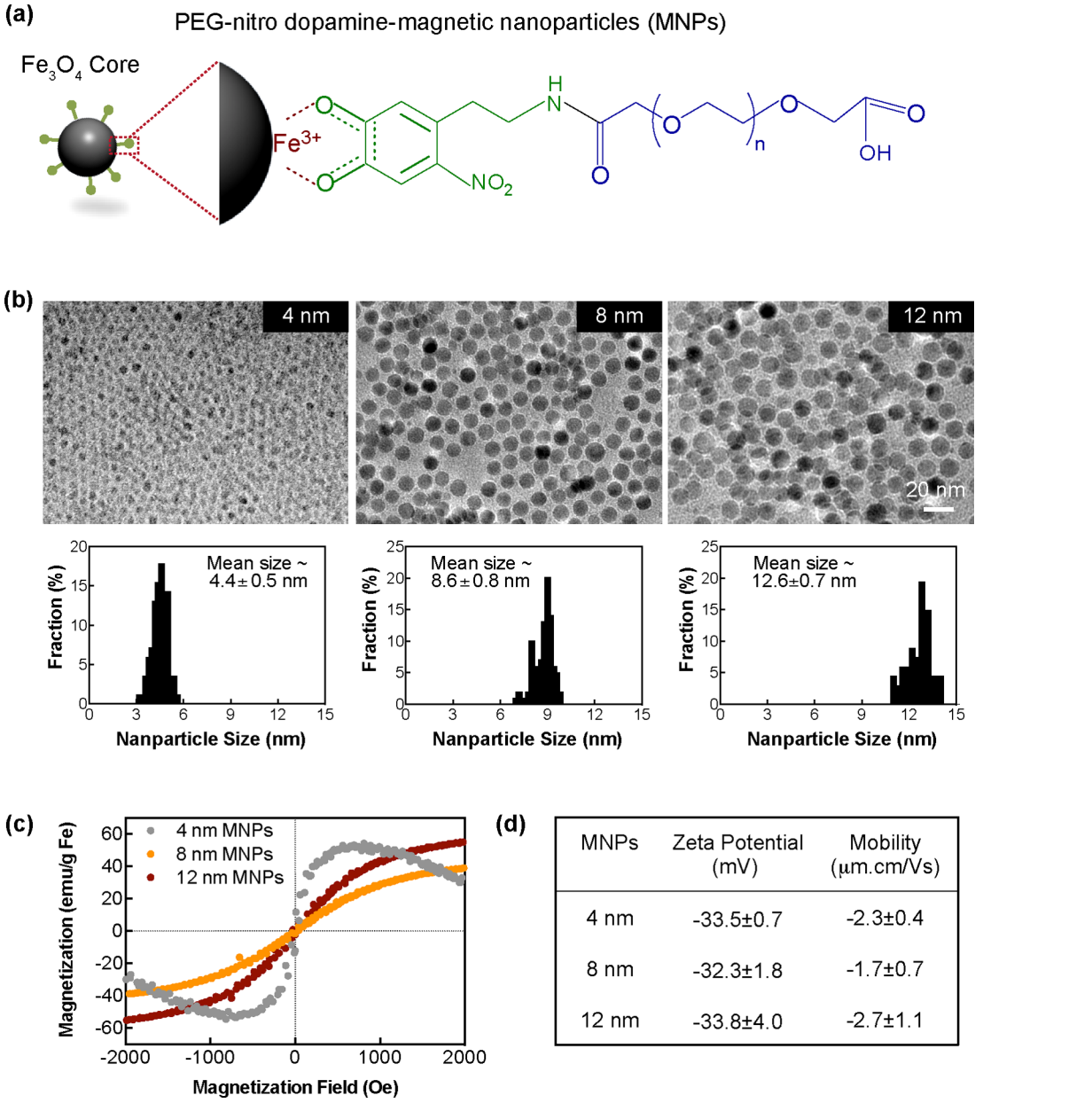

MNPs	Zeta Potential (mV)	Mobility (μm.cm/Vs)
4 nm	-33.5±0.7	-2.3±0.4
8 nm	-32.3±1.8	-1.7±0.7
12 nm	-33.8±4.0	-2.7±1.1

Figure 1. Synthesis and characterization of surface functionalized MNPs. (a) Oleic acid coated MNPs were decorated with nitro-dopamine anchored PEG diacid (COOH-PEG-COOH) using EDC-NHS chemistry. (b) TEM images of MNPs with different diameter and size distribution. (c) SQUID data of MNPs with different sizes indicating superparamagnetic characteristics. (d) Zeta potential and electrophoretic mobility of MNPs indicate highly stable nanoparticles in aqueous solution.

mechanical stiffness 2- to 3-fold at higher nanomaterial concentrations (3−20 mg/mL).[20,21] Despite these advances, collagen-based hydrogels are still not extensively used to engineer mechanically stiff tissues that can undergo plastic deformation and remain hydrated to support cellular infiltration.

Here, we report a highly efficient method to reinforce collagen-based hydrogels using extremely low concentrations (5 μg/mL) of a nanoparticulate-reinforcing agent that acts as a cross-link epicenter. We hypothesize that the cross-linking of multiple polymeric chains to the nanoparticle surface will provide control over the physical properties of the hydrogel network attribute. It is also expected that the mechanical stiffness of the nano-engineered hydrogel can be tailored simply by manipulating the size of the nanoparticulate-reinforcing agent, as well as the concentrations of the nanoparticles and polymer. It is expected that due to the facile approach to tune the mechanical properties without changing the chemistry of the polymer network, these nanoengineered hydrogels could be used to decouple the role of biomaterials chemistry and structure with cellular behavior. These nanoengineered hydrogels may have broad utility for various biomedical applications, including use as tissue-engineered scaffolds and cell/protein delivery vehicles.

RESULTS AND DISCUSSION

Synthesis and Characterization of Nanoparticle Cross-Linker. To develop the chemically reinforced nanocomposite networks, oleic acid coated iron oxide (Fe_3O_4) MNPs with three different sizes (4, 8, and 12 nm) were synthesized using methods reported in the literature.[23−25] The surface of the MNPs was modified with nitro-dopamine. Subsequently, poly(ethylene

DOI: 10.1021/acsnano.5b03918
ACS Nano 2016, 10, 246−256

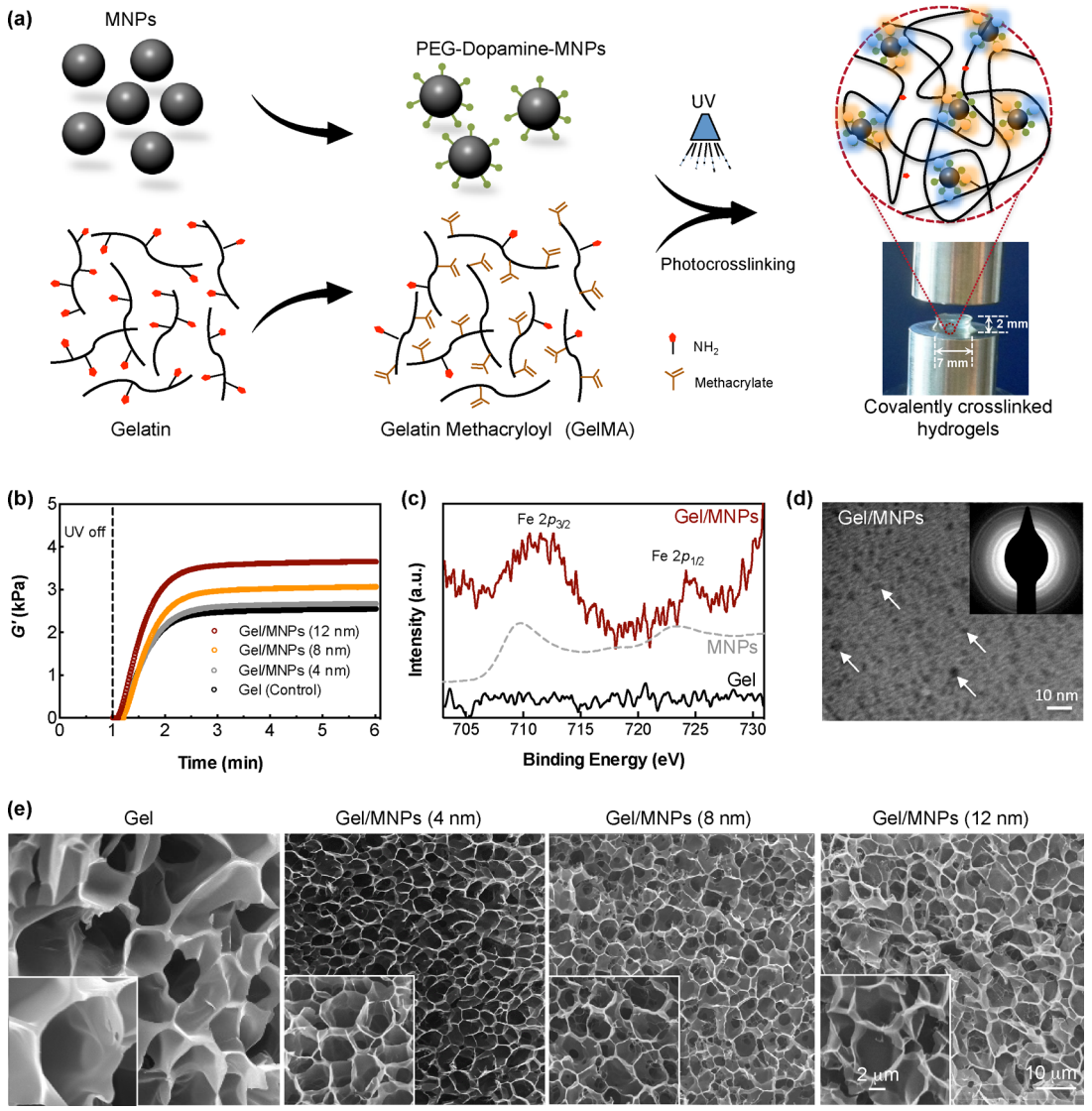

Figure 2. Synthesis of MNP-reinforced nanocomposite hydrogels. (a) Nanocomposite hydrogels were synthesized by combining PEG-dopamine-MNPs with GelMA and exposing it to UV radiation in the presence of a photoinitiator to obtain covalently cross-linked network. (b) Cross-linking of the prepolymer solution was monitored using UV rheology. After the UV radiation was turned on, a significant increase in the modulus of the prepolymer solution was observed, indicating the formation of a cross-linked network. (c) The presence of MNPs within nanocomposite network was determined from XPS. (d) TEM images of nanocomposite show uniform distribution of MNPs within GelMA matrix. Inset shows the electron diffraction pattern. (e) SEM micrographs of the nanocomposites indicate the formation of highly porous and interconnected networks.

glycol) (PEG) diacid was conjugated *via* carbodiimide-*N*-hydroxysuccinimide (EDC-NHS) chemistry,[26−28] as shown in Figures 1a, S1 and S2. Transmission electron microscope (TEM) images indicate the formation of monodisperse MNPs with sizes of 4.4 ± 0.5, 8.6 ± 0.8, and 12.6 ± 0.7 nm (Figure 1b). According to the magnetization profiles (M-H), the MNPs were superparamagnetic, as no hysteresis was observed (Figure 1c). The 12 nm MNPs had the maximum magnetization of 65 emu/g at 2 kOe. The 4 nm MNPs exhibited higher magnetization than 8 nm, likely due to the smaller-sized particles being able to easily aggregate in aqueous media. The magnetization profiles also indicated that adding the nonmagnetic coating (*i.e.*, the nitrodopamine-PEG ligand) onto the MNP surfaces reduced the absolute magnetization values of Fe_3O_4. The coating is also responsible for diamagnetic characteristics at higher fields, which were more pronounced in the 4 nm MNPs. The zeta potential and electrophoretic measurements of the MNPs (Figure 1d) indicated high stability of the nanoparticles in aqueous solvent, which can be attributed to the presence of the hydrophilic PEG chains on the nanoparticles.

Reinforcing Hydrogels with Nanoparticle as a Cross-Link Epicenter. To fabricate nanocomposite hydrogels, denatured collagen (gelatin) was selected as the base polymer. Notably, gelatin contains cell-binding domains and can be easily modified to obtain covalently cross-linked hydrogels that mimic the native tissue microenvironment.[18] Briefly, the primary amine groups present on the gelatin backbone were partially modified with methacrylate groups to obtain photo-cross-linkable gelatin methacryloyl (GelMA), according to previously published reports.[18,22] The degree of methacrylation was 80%, indicating that 80% of amine groups present on gelatin backbone were transformed into a methacrylamide group.[18,22] Covalently cross-linked gelatin hydrogels (Gel) were produced by exposing a prepolymer solution of 5 wt % GelMA to ultraviolet (UV)

DOI: 10.1021/acsnano.5b03918
ACS Nano 2016, 10, 246−256

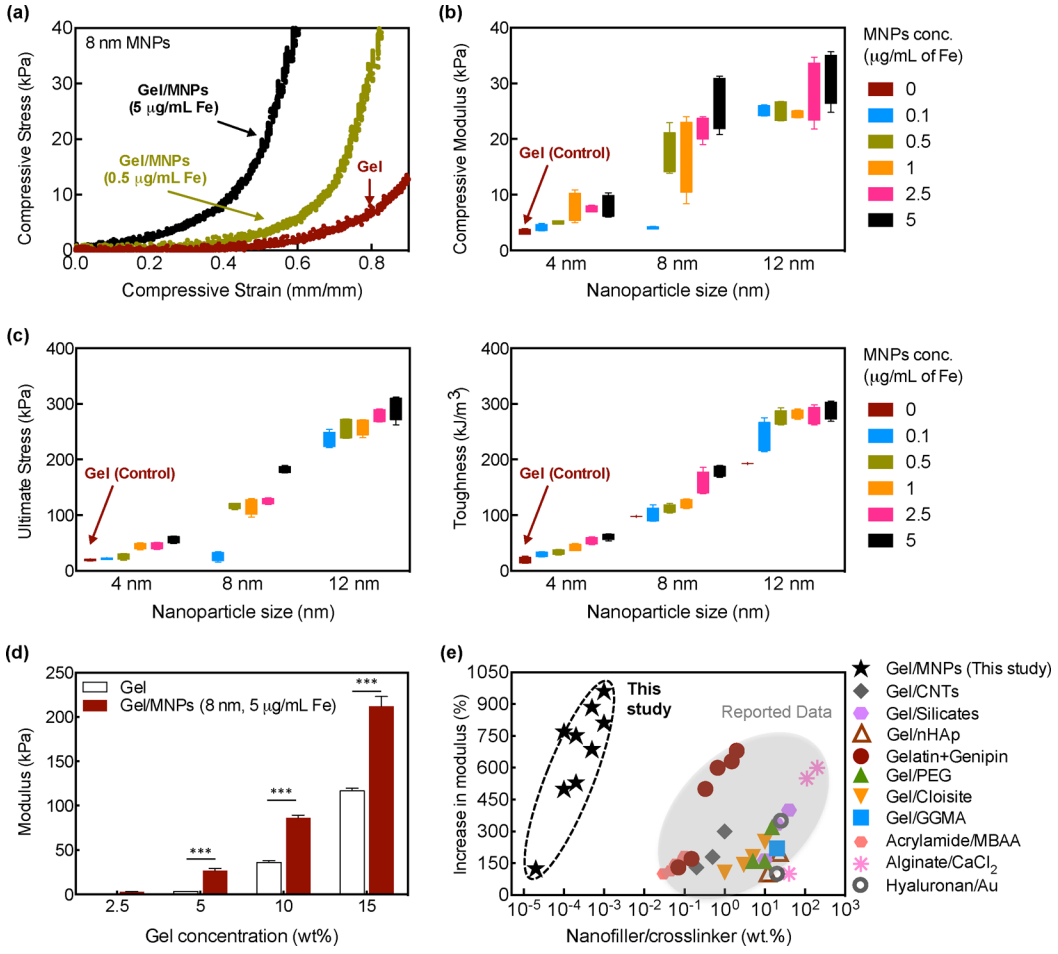

Figure 3. Effect of MNPs on the mechanical properties of covalently cross-linked hydrogel networks. (a) Representative stress−strain curves for nanocomposites loaded with 8 nm MNPs (0.5 and 5 μg/mL of Fe). Box plot of nanocomposites reinforced with different concentrations of 4, 8, and 12 nm MNPs for (b) compressive moduli, (c) ultimate stress and toughness. (d) The effect of polymer concentration (2.5, 5, 10 and 15%) on compressive modulus of nanocomposite reinforced with 8 nm MNPs (5 μg/mL Fe). (Error bars not visible in some plots; they are too small). (e) The comparative chart of the moduli of various nanocomposite hydrogels: Gel-CNTs,[20,21] Gel/Graphene,[19] Gel/Silicate,[22] Gelatin + Genipin,[31] Gel/PEG,[32] Gel/nHAp,[33] Gel/Cloisite,[34] Gel-GellanGum(GGMA),[35] Acrylamide/MBAA,[17] Alginate/$CaCl_2$,[36] Hyaluronan/Au.[37]

radiation (320−500 nm; 30 mW/cm^2) in the presence of a photoinitiator (0.5 wt % Irgacure 2959). Nanocomposite hydrogels were fabricated (Figure 2a) by combining 5 wt % GelMA prepolymer solution with different sizes (4, 8, and 12 nm) and concentrations of the functionalized MNPs (0.1−5 μg/mL of iron (Fe)) and then performing UV cross-linking.

Cross-linking of the MNP-reinforced nanocomposite hydrogels (5 μg/mL of Fe in 50 mg/mL GelMA) was evaluated by using a rheometer to monitor shear modulus evolution over time during photo-cross-linking (Figure 2b). As expected, the uncross-linked prepolymer solution containing GelMA and MNPs exhibited a low storage modulus (G') before UV exposure (<1 min). After UV exposure (>1 min), which initiated crosslinking of polymer network, a sudden increase in G' was observed, indicating the formation of a covalently cross-linked network. In general, G' reached a plateau after 1 min of UV exposure, indicating that the network was fully cross-linked. However, the final storage modulus (G') obtained was strongly influenced by the size of the functionalized nanoparticles, suggesting interactions between the ligands present on the MNPs and the collagen. In addition, we observed that the incorporation of MNPs resulted in enhanced network stability as determined from frequency sweep and stress sweep data (Figures S3 and S4).

The presence of MNPs within the cross-linked Gel network was confirmed by X-ray photoelectron spectroscopy (XPS) (Figure 2c) and electron diffraction pattern (TEM) (Figure S5). The presence of peaks at ~712 and 724 eV corresponded to Fe $2p_{3/2}$ and Fe $2p_{1/2}$, respectively, in the nanocomposites; these peaks were absent in Gel hydrogels that did not contain MNPs. XRD data also indicate presence of MNPs within the cross-linked samples (Figure S5). The presence of MNPs in the prepolymer solution before photo-cross-linking was analyzed by TEM, which displayed the homogeneous distribution, indicating ultrastable suspension in prepolymer solution (Figure 2d). The nanoparticles are crystalline and hence they appear dark and can be seen easily in the lighter polymer background.

The morphological features of the Gel and Gel-MNP hydrogels were analyzed using scanning electron microscopy (SEM), and the results indicated a porous and interconnected network with pore sizes of 8−10 μm (Figure 2e), similar to previously published reports.[20,21] The addition of MNPs to Gel significantly reduced the pore size of the nanocomposite hydrogels, indicating an increase in cross-linking density. Thus, an increase in mechanical stiffness due to addition of MNPs can be expected. However, all the hydrogel showed highly porous and interconnected network, indicating their ability to support

DOI: 10.1021/acsnano.5b03918
ACS Nano 2016, 10, 246−256

nutrient and waste transfer. Furthermore, we investigated the effect of MNPs addition to Gel on hydration and degradation characteristics of hydrogel network. The addition of MNPs to the Gel hydrogels did not have a significant effect on the hydration and degradation profile (Figure S6).

Physical and Structural Characterization of Mechanically Stiff Nanocomposite Hydrogels. To investigate the influence of MNPs on mechanical properties, an unconfined compression test was performed on the nanocomposite hydrogels and compressive modulus was calculated from engineering stress−strain curve. The modulus calculated from the initial linear region (0.1−0.2 mm/mm strain) of the stress−strain curve of nonreinforced Gel hydrogels was observed to be 3.2 ± 0.5 kPa (Figure 3a), which is comparable to previously published reports.[19] The addition of nitro-dopamine functionalized MNPs to gelatin hydrogels resulted in a significant increase in mechanical stiffness compared to the Gel hydrogels (Figure 3b); the addition of 0.1, 0.5, 1, 2.5, and 5 μg/mL (Fe) of MNPs (8 nm) to Gel hydrogels increased the modulus to 4 ± 0.2, 16.9 ± 4.1, 17.3 ± 6.6, 22.2 ± 2.2, and 26.7 ± 4.7 kPa, respectively. A more than 8-fold increase in mechanical stiffness was observed by adding just 0.5 μg/mL of MNPs, which corresponded to a 10 000-fold lower concentration compared to the polymer concentration (50 mg/mL). It should be appreciated that the increase in mechanical stiffness and toughness can be controlled by modulating the density of the nitro-dopamine-PEG functionality on the MNP surfaces. Though smaller size of MNPs (4 nm) had larger net surface area, but due to inevitable aggregation, the possible number of available cross-linking points on nanoparticle surface was significantly lower compared to the larger MNPs (8 and 12 nm). The aggregation of smaller size nanoparticles was evident in magnetization data (Figure 1c). Thus, the addition of 5 μg/mL of 4 nm-MNPs resulted in a moderate 2.5-fold increase in modulus (7.8 ± 1.9 kPa) compared to Gel, whereas the addition of 12 nm-MNPs (5 μg/mL) resulted in ∼10-fold increase in modulus (31.25 ± 4.6 kPa) compared to Gel. A similar trend was observed in storage modulus when hydrogels was subjected to shear deformation (Figure 2b).

Moreover, similar trends were observed for ultimate stress and toughness (Figure 3c) with the change in nanoparticle size and concentration. The energy absorbed by the Gel hydrogel after 0.8 mm/mm strain was 16.9 ± 2.9 kJ/m^3. The addition of 0.5 and 5 μg/mL of MNPs (8 nm) to Gel resulted in increases in toughness to 113.7 ± 7.6 and 178.8 ± 8.3 kJ/m^3, respectively. The addition of 4, 8, and 12 nm MNPs at a concentration of 5 μg/mL resulted in 3-fold (61.5 ± 5.5 kJ/m^3), 11-fold (178.8 ± 8.3 kJ/m^3), and 17-fold (286.9 ± 13.6 kJ/m^3) increases in toughness, respectively. To confirm that amine groups present in Gel are interacting with MNPs, we replaced GelMA with poly(ethylene glycol) (PEG) diacrylate with the functionalized MNPs (0.1−5 μg/mL of iron (Fe)) (Figure S7). No significant increase in mechanical stiffness was observed indicating amines present on GelMA play a critical role in chemical conjugation.

This approach of reinforcing Gel hydrogels was expanded to hydrogels prepared from different concentrations of GelMA. By changing the GelMA concentration, the number of available unreacted $-NH^{3+}$ and methacrylate groups would increase or decrease with the change in polymer concentration. We used 5 μg/mL of 8 nm-MNPs to reinforce covalently cross-linked hydrogels comprising 2.5, 5, 10 and 15% GelMA (Figure 3d). A significant increase in mechanical stiffness was observed for all compositions when MNPs were added. Almost a 10-fold increase in modulus was observed in nanocomposites containing 2.5 and 5% GelMA, whereas around a 2.5-fold increase in modulus was observed at higher GelMA concentration. Since the MNP concentration was held constant, the cross-linking sites present on MNPs were exhausted at higher GelMA concentration. This result indicates that by changing the concentration of polymer and nanoparticles, a range of mechanical stiffness can be obtained.

Compared to other reported stiff hydrogels, the amount of nanoparticles (or cross-linker) used here is 2−3 orders of magnitude lower. Even at a 10 000-fold lower concentration of nanoparticles compared to polymer, we were able to achieve more than a 10-fold increase in mechanical stiffness. This is mainly due to the fact that each nanoparticle acts as cross-link epicenter, and the nanoparticle surface covalently interacts with multiple polymeric chains to form highly cross-linked network. Furthermore, we believe this concept can easily be generalized for different shaped nanoparticles such as one-dimensional (1D), two-dimensional (2D), and three-dimensional (3D) nanoparticles to further enhance the stiffness of polymeric networks.[29,30] As the proposed approach is surface-mediated, by increasing surface roughness or features, it is possible to fine-tune the mechanical properties of nanocomposites. Notably, some of the other cross-linking techniques that have been used to achieve mechanically stiff hydrogels (*e.g.*, double-network hydrogels,[11] supramolecular or topological hydrogels,[12] microsphere-cross-linked hydrogels,[13] nanoclay-cross-linked hydrogels,[14,15] and hybrid physical/chemical cross-linked hydrogels[17]) have also not been able to provide a 10-fold increase in stiffness with such low concentrations of reinforcing agents.

To illustrate the significance of this result, the comparative plot Figure 3e shows the percentage increase in moduli with respect to nanofiller/reinforcing agent/cross-linker concentration in Gel hydrogel systems including Gel-CNTs,[20,21] Gel/Graphene,[19] Gel/Silicate,[22] Gelatin + Genipin,[31] Gel/PEG,[32] Gel/nHAp,[33] Gel/Cloisite,[34] Gel-GellanGum(GGMA),[35] Acrylamide/MBAA,[17] Alginate/$CaCl_2$,[36] Hyaluronan/Au.[37] For example, the addition of CNTs to Gel hydrogels resulted in merely 3-fold increase in hydrogel modulus.[20] 2D nanomaterials such as graphene did not significantly change the compressive modulus when incorporated within Gel, and instead simply acted as a filler.[19] When the surface of graphene oxide was modified with methacrylate groups, its interactions with Gel were increased and resulted in a 2- to 3-fold increase in stiffness.[38] Another type of 2D nanomaterial that has a charged surface (synthetic silicates) resulted in a 4-fold increase in stiffness due to the enhanced nanoparticle−polymer interactions.[22] Some other attempts to increase the mechanical stiffness of Gel hydrogels include the formation of semi-interpenetrating networks using Gellan Gum[35] and PEG;[32] these approaches also resulted in moderate increases in stiffness. Comparing to the existing literature, the present study clearly highlights that dopamine functionalized MNPs are efficient in increasing the mechanical robustness by 10-fold at ultralow (10 000-fold less) nanoparticle concentrations, which is superior to many alternatives at similar relative concentrations.

Chemical Characterization of Reinforced Hydrogel Network. The increase in mechanical stiffness can be attributed to covalent cross-linking between gelatin backbones and surface functionalized MNPs. Being photoactive, nitro-dopamine (λ_{abs} = 310 nm) present on MNPs might act as a cross-link epicenter. The role of surface functionalized MNPs in reinforcing the hydrogel network was probed using XPS. The change in binding energies (B.E.) for nitrogen (N 1s), carbon (C 1s) and oxygen

DOI: 10.1021/acsnano.5b03918
ACS Nano 2016, 10, 246−256

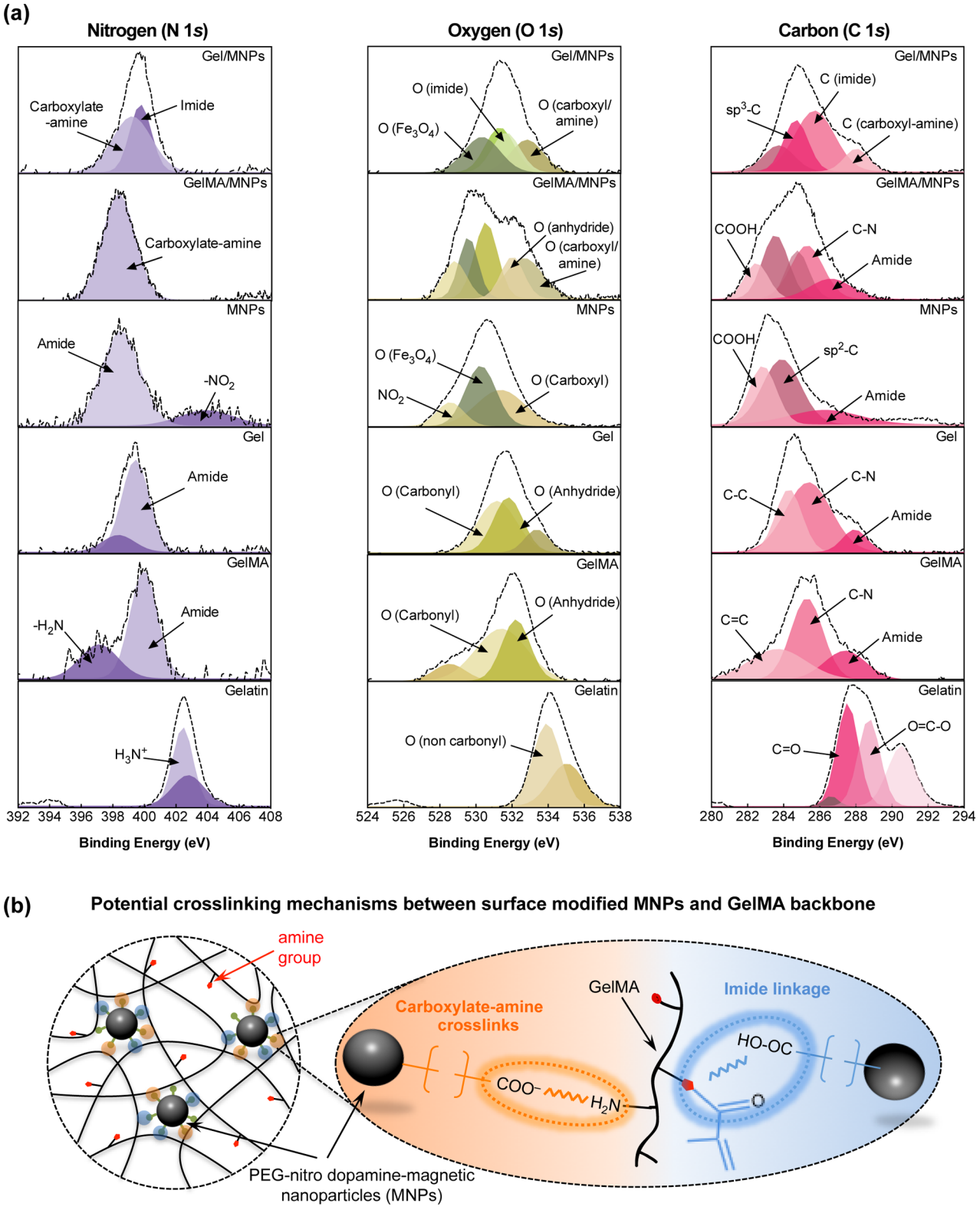

Figure 4. Chemical interactions between nanoparticle and polymer. (a) High-resolution X-ray photoelectron spectra of Gelatin, GelMA (prepolymer), Gel (*i.e.*, cross-linked GelMA), MNPs, GelMA/MNPs (*i.e.*, prepolymer solution), and Gel/MNPs (cross-linked nanocomposite). The peaks for nitrogen (N 1s), oxygen (O 1s) and carbon (C 1s) atoms have been deconvoluted into curve components, which are shown underneath the experimental data points (dotted lines). (b) Proposed cross-linking mechanism between surface modified MNPs and polymer backbone (GelMA).

(O 1s) for gelatin, GelMA, Gel (*i.e.*, cross-linked gelatin), MNPs, GelMA/MNPs and Gel/MNPs are shown in Figure 4a and Table S1. The N 1s peak for gelatin appeared at around 402.5 and 402.8 eV due to presence of free amine (NH_3^+) on polymer backbone. The methacrylation of gelatin gives rise to amide (399.8 eV) along with primary amine (397 eV) peaks in PBS. After photo-

DOI: 10.1021/acsnano.5b03918
ACS Nano 2016, 10, 246−256

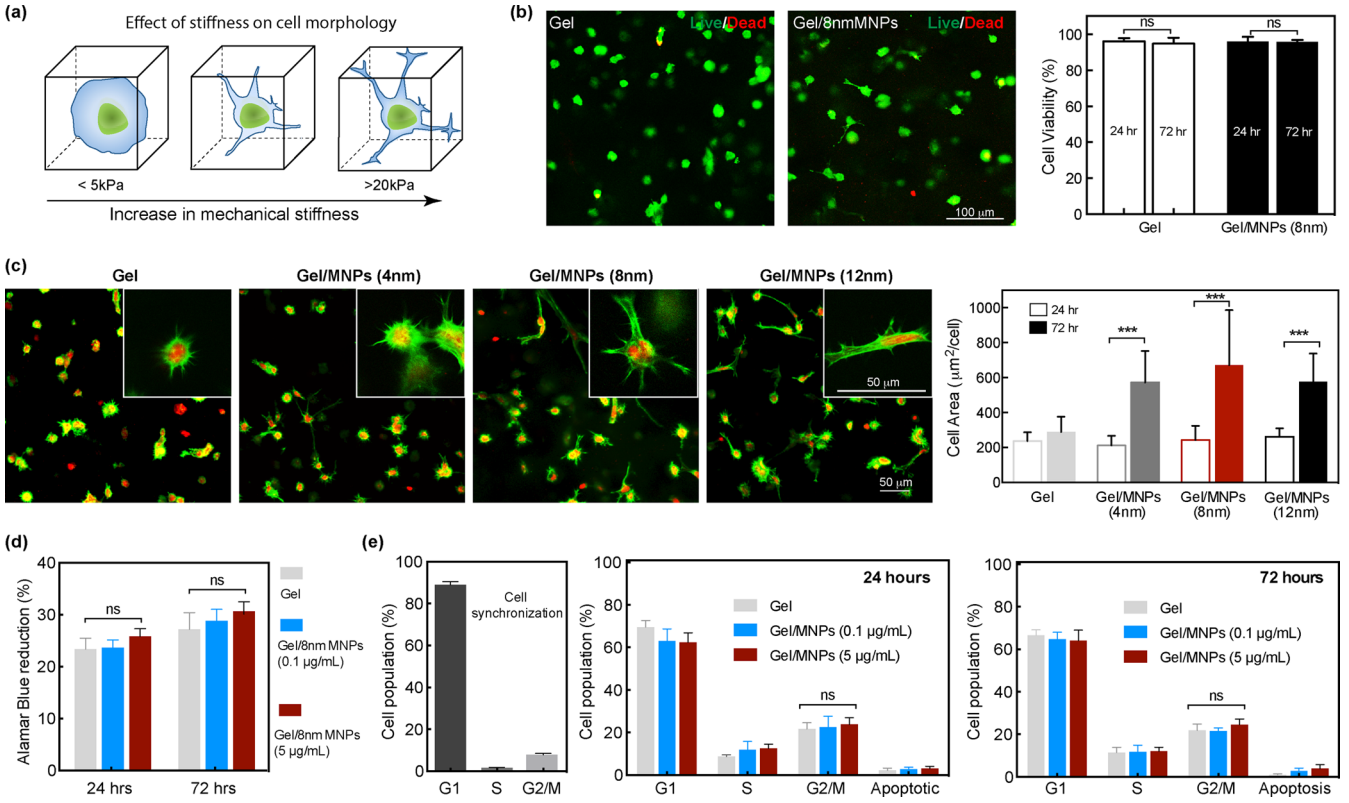

Figure 5. Effect of mechanically stiff nanocomposite hydrogels on cellular behavior. (a) The addition of nanoparticles result in significant increase in mechanical stiffness of hydrogel matrix and it is expected to influence cell morphology. (b) Due to facile fabrication process, encapsulated cells showed high viability after 24 and 72 h. (c) Cell shape was significantly influenced due to matrix stiffness. Cells encapsulated within Gel showed circular morphology, while cells in nanocomposite showed elongated and spread morphology, indicating that cells sense and respond to external stimuli. (d) Cells seeded on nanocomposite hydrogel readily proliferated as determined by Alamar blue assay. (e) Cells were synchronized *via* serum reduction for a 24 h period. No significant effect of stiffness was observed in cell cycle.

cross-linking of the methacrylate groups, the associated N 1s peak was shifted marginally toward lower binding energy due to the change in vicinity. The N 1s peaks at 398.4 and 403.8 eV in MNPs are attributed to the amide and nitro groups, respectively, of the nitro-dopamine-PEG. In the prepolymer solution consisting of GelMA and MNPs; amide and amine peaks would be expected to appear at 399.8 and 397 eV, respectively (due to GelMA). Instead, a new peak with considerable shift in the primary amine position, at 398.4 eV emerged, indicating a strong carboxylate-amine interaction in the prepolymer solution of GelMA and MNPs. After UV cross-linking, peak splitting was observed in Gel/MNPs, suggesting the shift in carboxylate-amine cross-linking (399.1 eV) and the formation of imide linkages (399.7 eV), due to interactions between the amide groups of the methacrylated polymer chains and the carboxylates of the MNPs. The peak associated with nitro groups of the MNPs was not detected in the prepolymer solution (GelMA+MNPs), likely due to the ultralow concentration.

Comparison of the O 1s peaks for gelatin and GelMA indicated the presence of noncarbonyl oxygen (534 eV) that was transformed into carbonyl (531.5 eV) and anhydride (532.1 eV) after methacrylation. After UV cross-linking, the carbonyl and anhydride peaks in Gel were shifted due to change in vicinity in the neighboring atoms. An additional O 1s peak was observed for Gel at B.E. 533.4 eV, perhaps due to ester formation. The oxygen peaks observed at 530.1, 528.4, and 531.4 eV in MNPs correspond to iron oxide, nitro-dopamine, and carboxylates, respectively. In the prepolymer solution of GelMA and MNPs, the iron oxide, nitro-dopamine, and carboxylate peaks were shifted and peaks corresponding carboxylate-amine interactions (532.6 eV) appeared, confirming the strong interactions of GelMA and MNPs. Upon UV exposure, a strong peak corresponding to the imide formation between the amides of GelMA and carboxylate groups of MNPs was observed.

The C 1s peaks for gelatin show the presence of carbonyl C═O and carboxyl (O−C═O) peaks at 287.5 and 288.8 eV, respectively. Methacrylation of the primary amines of gelatin resulted in the formation of C═C (283.8 eV) and amide (288.2 eV). After UV cross-linking of GelMA, a peak appeared at 284.4 eV, corresponding to the C−C bond formed by polymerization. In MNPs the carbon positions corresponding to COOH and amide were observed at 282.7 and 286.8 eV, respectively. In the prepolymer solution (GelMA + MNPs), all the peaks corresponding to GelMA and MNPs were observed. After UV cross-linking, peaks at 288.1 and 285.8 eV indicate the formation of carboxylate-amine and imide interactions.

Overall, the XPS data confirmed that interactions occurred between the MNPs and polymer in the nanocomposite hydrogels and provided further evidence for MNPs acting as focal points from which polymeric cross-linking originated. The cross-linking mechanism obtained from XPS data indicates the formation of "imide" bonds as well as the presence of "carboxylate-amine" interactions between nanoparticles and polymer (Figure 4b). The ability of MNPs to provide multiple cross-linking points and its ability to covalently interact with polymer chains at multiple location are believed to be the

DOI: 10.1021/acsnano.5b03918
ACS Nano 2016, 10, 246−256

underlying mechanism for the observed increases in mechanical stiffness.

Effect of Mechanically Stiff Nanocomposite Hydrogels on Cellular Behavior. The ability to encapsulate cells and subsequent support proliferation is an important requirement of a tissue engineered scaffold. Cellular behavior of encapsulated cells is regulated *via* multiple microenvironmental cues including mechanical stiffness, presence of cell adhesion ligands, ECM proteins and soluble factors.[39,40] Among these external signals, mechanical stiffness of the hydrogel scaffolds plays an important role in governing cells shape (Figure 5a). Various reports demonstrated that cell shape profoundly impacts the cell fate *via* intracellular signaling.[41] This ability of cells to sense and respond to external mechanical stimuli is extensively investigated for regenerative engineering. Moreover, ECM stiffness can also direct the differentiation of encapsulated stem cells toward certain tissue lineages. For example, soft hydrogels (<5 kPa) support circular morphology of encapsulated cells and support adipogenic/chondrogenic differentiation, while stiff hydrogels (>20 kPa) facilitate cells spreading and formation of strong cytoskeleton and induces osteogenic differentiation.[41,42] Here, we demonstrated that surface-modified MNPs can reinforce GelMA by up to 10-fold at far lower concentrations (10 000-fold) nanoparticle concentrations. These ultralow nanoparticle concentrations modify matrix stiffness (~3−30 kPa) with minimal direct interactions with cells. Thus, it is expected that this nanocomposite hydrogel system can be used to delineate the effect of matrix stiffness and engineer cell-matrix interactions.

Due to facile cross-linking process, we can encapsulate human bone marrow stem cells (hMSCs) and murine-derived preosteoblasts (MC3T3s) within the nanocomposite hydrogel network. Cells survive the gelation process and maintain high viability after 24, 48, and 72 h, as evident by high number of live (green) cells compared to dead cells (red) (Figures 5b, S8 and S9). The effect of matrix stiffness was observed on cell spreading. After 24 h, encapsulated cells showing circular morphology were observed in Gel and nanocomposite hydrogels. After 72 h, no significant change in cell spreading was observed (Figure 5c) in Gel. The addition of 4, 8, and 12 nm MNPs to Gel results in significant increase in cell spreading. The projected cell area was calculated from the confocal images, quantitatively demonstrating the effect of matrix stiffness on cells spreading (Figure 5c). The effect of matrix stiffness was also investigated by determining the circularity index (1 ~ circular and <1 ~ elongated) of encapsulated cells. Cells encapsulated within Gel (0.6 ± 0.2) and Gel/MNPs (12 nm) (0.3 ± 0.1) showed significant difference in circularity index. In addition, well-organized actin cytosketon was observed in nanocomposite hydrogel with high stiffness (>20 kPa).

The metabolic activity of encapsulated cells was investigated using Alamar Blue assay and cell cycle analysis. The addition of nanoparticles does not result in any significant change in metabolic activities of cells, indicating high cytocompatibity of cross-linking process (Figure 5d). To investigate proliferative capacities of the nanocomposite hydrogels, cell cycle analysis *via* flow cytometry was performed. Initially, cells were synchronized *via* serum reduction for a 24 h period, enabling presentation of a more robust material effect after cell seeding. Incubation on the materials for 24 and 72 h provided ample time for trends to emerge among cell populations (Figure 5e). Cells seeded on the nanocomposite hydrogels began to display enhanced proliferation after 24 and 72 h. A significant increase in the G_2/M population was observed, signifying a shift into a higher proliferative capacity. As expected, this was accompanied by a decrease in the G_1/G_0 population as cells entering a mitotic state. RGD sequences within the natural polymer promote cellular adhesion and subsequent cellular spreading, likely leading to the augmentation of cell numbers. Overall, the presented data suggest a promising future for the use of epicenter cross-linked nanocomposite hydrogels in cell and tissue engineering, and *ex vivo* cell culture models. Future investigations will focus on understanding the effect of mechanical stiffness of nanocomposite hydrogels on cellular behavior.

CONCLUSIONS

We have successfully synthesized mechanically stiff collagen-based hydrogels by incorporating a 10 000-fold lower concentration of nanoparticles without sacrificing pore morphology and interior hydrogel architecture. The chemical reinforcement with nitro-dopamine-PEG functionalized nanoparticles resulted in a 10-fold increase in mechanical stiffness and a 20-fold increase in toughness. The increase in mechanical stiffness of the nanocomposite hydrogels is due to the multifunctional nature of the nanoparticles, which act as cross-link epicenters. The mechanical stiffness of the nanoengineered hydrogel can be tailored between 0.2 and 200 kPa simply by manipulating the size of the nanoparticles (4, 8, and 12 nm), as well as the concentrations of the nanoparticles and polymer. Moreover these nanoengineered hydrogels are highly elastomeric and can sustain more than 90% compressive strain with minimal plastic deformation. Due to facile cross-linking process, high viability of encapsulated cells was observed. In addition, encapsulated cells were able to sense and respond to external mechanical stimuli. The ultralow nanoparticle concentrations required to modify the matrix stiffness can be used to understand and direct cellular fate. Overall, these nanoengineered hydrogels can be used to engineer mechanically stiff networks for biomedical applications including tissue-engineered scaffolds, drug delivery vehicles, bioactuators, and sensors.

METHODS

Synthesis of Magnetite Nanocrystals. For the synthesis of 4 nm magnetite nanocrystals, the protocol established by Sun *et al.* was used.[43] In a typical reaction, the precursors iron(III) acetylacetonate (*ca.* 1.41 g), lauric acid (*ca.* 2.40 g), hexadecanediol (*ca.* 5.17 g), dodecylamine (2.76 mL) (all procured from Sigma) were dissolved altogether in 40 mL of benzyl ether (bp 298 °C) and heated to 180 °C for about 4 h under N_2 blanket. The reaction chamber was raised to 295 °C slowly and maintained for 10 min. The formed nanocrystals were of the size approximately 4 nm with oleic acid coated onto it.

For the synthesis of 8 and 12 magnetite nanocrystals, we followed the standard methodology based on the high temperature decomposition of iron oleate complex (Figure S1).[24] In brief, 40 mmol of ferric chloride hexahydrate ($FeCl_3 \cdot 6H_2O$, procured from Sigma) and 120 mmol of sodium oleate (procured from Fluka) dissolved in the mixture solvent of ethanol, water and hexane was heated at 70 °C for about 4 h under N_2 blanket. The thus obtained complex was properly washed with ultrapure water and the excess of hexane was evaporated to get wax-like solid product. In the next step, the calculated amount of the obtained complex (5.815 g) was dissolved in 40 mL of 1-octadecane (bp 317 °C) and 1.08 mL of oleic acid and raised to 315 °C at controlled rate of 3.3 °C/min and maintained for 10 (or 15) min to achieve hydrophobic oleic acid functionalized Fe_3O_4 nanocrystals of sizes 8 (or 12 nm) respectively.

Hydrophilic Fe_3O_4 MNPs by Nitro-Dopamine-PEG. The oleic acid coated hydrophobic Fe_3O_4 nanocrystals were made aqueous stable by replacing the long aliphatic chain molecules from the surface and stabilizing them by functionalizing with PEG diacid (procured from Millipore, USA) *via* strong anchoring ligand of nitro-dopamine. The

DOI: 10.1021/acsnano.5b03918
ACS Nano 2016, 10, 246−256

dual hydroxyl groups of the catechol part of nitro-dopamine get oxidized easily and bind with the Fe^{3+} onto the nanoparticle surfaces and hence establish a robust and highly sustainable nanoparticles under physiological conditions.[25,26] The presence of additional nitro group ($-NO_2$) facilitates electron deficiency in the benzene ring and thus helps easy oxidation of hydroxyl groups. Furthermore, the surface was modified with PEG-diacid using simple EDC-NHS chemistry wherein the one end carboxylate group of PEG undergoes esterification and binds with nitro-dopamine, while the other end extends in water and provides ultrastable aqueous suspension. The detail mechanisms of this chemistry is described in the Supporting Information (Figure S2). In typical laboratory procedure for the ligand solutions, 55.8 mg of nitro-dopamine and 144 mg of PEG diacid were dissolved in 15 mL of chloroform. The prepared solution was subsequently mixed with $NaHCO_3$ (100.8 mg), NHS (27.6 mg), and DCC (49.5 mg, in place of EDC) solution prepared prior in 30 mL DMSO. The entire mixture was purged with N_2 and magnetically stirred for next 24 h. About 5 mg of hydrophobic magnetite precipitated into ethanol was added into the ligand solution and the mixture was sonicated for next 24 h to achieve phase-separated nanoparticles which was redispersed in water to achieve aqueous suspension. The PEG diacid was first made to react with carbodiimide groups containing DCC (dicyclohexylcarbodiimide) in slightly basic medium which replaces H^+ from one of the carboxylic acids and forms the intermediate containing isourea group which can easily be replaced by NHS (*N*-hydroxysuccinimide) to activate esterification of the PEG molecules. The activated ester groups have the affinity to bind with amine, and hence, after addition of nitro-dopamine, the solution was stirred for about 24 h to get the nitro-dopamine-PEG ligand solution. The prepared oleic acid coated Fe_3O_4 nanocrystals were then added into this prepared solution and the mixture was sonicated for another 24 h to get the aqueous stable MNPs.

Synthesis of Methacrylated GelMA. Gelatin has abundance of free amine groups in the form of lysine which provide easy acrylation sites. Gelatin methacylate (GelMA) with 80% methacrylated degree was prepared by acrylation of pendent amine groups initiated by 2-methacrylic anhydride (MA) in PBS at elevated temperature, according to previously published protocols.[18] In a typical experiment, 10 g of gelatin (extracted from porcine skin, sigma) was dissolved in 100 mL of PBS at 60 °C for an hour under vigorous stirring using magnetic bar. Eight milliliters of MA was added dropwise thereafter, and the solution was allowed to stir for another 3 h. The reaction was finally terminated by adding excess of preheated PBS into the solution. The prepared sample was collected and dialyzed against ultrapure water (18.2 MΩ·cm) at 40 °C in a cellulose dialysis bag (Mol. wt. cutoff ~12 kDa) for a week before freeze-drying and lyophilizing to get the GelMA in white solid foam form. The GelMA prepared this way was roughly 80% acrylated.

Preparation of UV Cross-Linked Gel Discs. Photo-cross-linked 5% (w/v) GelMA and GelMA incorporated with MNPs (GelMA + MNPs) with varied MNPs concentrations from 0.1 to 5 μg/mL Fe of different sizes (4, 8, and 12 nm) were prepared using 0.5% irgacure 2959 (Sigma) as photoinitiator (PI). Typically, 100 μL of GelMA (5 mg) solution with PI (0.5 mg) in aqueous medium was used to expose UV light (30 mW/cm^2) for 60 s to get a disc-shaped gel of the dimensions 7 mm (diameter) × 2 mm (thickness) and maintained in 1 mL of DPBS overnight before using them for further experiments and measurements. All the measurements were carried out using five replicates unless otherwise stated.

Physical and Chemical Characterizations. The zeta potential and electrophoretic mobility of the GelMA and GelMA/MNPs prepolymer solutions were measured at 25 °C using a Zetasizer (Malvern Instrument, U.K.) equipped with a He−Ne laser. Transmission electron microscopy (TEM) was performed using JEOL-JEM 2010 (Japan) at an accelerating voltage of 200 kV on carbon grid. The surface morphology of the nanocomposite hydrogels was evaluated using scanning electron microscopy (SEM, FEI Quanta 600 FE-SEM, USA, fitted with Oxford EDS system) at an accelerating voltage of 20 kV. In brief, to prepare sample for SEM, the nanocomposite hydrogels were frozen using liquid nitrogen and then lyophilized for 3 days to obtain dried sample. The dried nanocomposite samples were sputter coated with Au/Pd up to a thickness of 8 nm before being mounted onto the specimen stage for imaging. The pore diameters were analyzed using ImageJ software (National Institutes of Health, USA).

The mechanical properties of the Gel and nanocomposite hydrogels were determined using a mechanical tester (Xpert 7600, ADMET, USA). Hydrogels ($n = 6$) were incubated in PBS for 24 h before testing. A uniaxial compression test was performed on the cylindrical samples (6 mm × 2 mm) at a strain rate of 1 mm/min. The compressive modulus was calculated from the slope in the toe region corresponding to 0.10−0.20 strain in engineering stress−strain curve (force divided by original cross-section area). The viscoelastic behavior of the hydrogels was evaluated using MCR Rheometer (Anton Paar, USA) equipped with 50 mm flat geometry and a gap of 50 μm.

The swelling behavior (or hydration degree) of the nanocomposites were also studied and calculated according to the formula mentioned below. The samples were soaked in 1× PBS (pH 7.4) and the wet weight (M_o) was measured; then the samples were lyophilized for 24 h to measure the dry weight (M_t).

$$\text{Hydration degree} = \frac{M_o - M_t}{M_t} \times 100 \quad (1)$$

For enzymatic degradation of the samples, gel discs were placed in 1 mL freshly prepared 2.5 units/mL collagenase type II (procured from Worthington Biochemicals, USA) solution in PBS at 37 °C. Weight loss was monitored until the gels were completely decomposed (Figure S6).

The formation of dual cross-linked network between gelatin and MNPs coated with nitro-dopamine-PEG diacid was analyzed using X-ray photoelectron spectroscopy (XPS) (Omicron XPS/UPS system with Argus detector). The changes in binding energies (B.E.) for nitrogen (N 1s), carbon (C 1s) and oxygen (O 1s) and for gelatin, GelMA, Gel (cross-linked gelatin), MNPs, GelMA/MNPs and Gel/MNPs were recorded and all the raw data were processed and deconvoluted by CasaXPS multiple peak fit software version 2.3.15. The references for XPS interpretations are listed in Table S1. Furthermore, the semicrystalline property of Gelatin was utilized to confirm the cross-linking of Gel/MNPs nanocomposites. X-ray diffraction pattern (Bruker, USA) of both gelatin and nanocomposite recorded showed the forward angle shift in the characteristic peak positions as shown in Figure S5.

***In Vitro* Cell Studies.** Human Mesenchymal Stem Cells (hMSCs) were obtained from Texas A&M Health Science Center College of Medicine Institute for Regenerative Medicine at Scott & White. Murine-derived preosteoblasts (NIH MC3T3 E1−4, ATCC, USA) and hMSCs were cultured in normal growth media (Alpha MEM, Life Technologies, USA), supplemented with 10% FBS (Life Technologies, USA) and 1% penicillin/streptomycin (100 U/100 μg/mL; Life Technologies, USA) at 37 °C with 5% CO_2. The nanocomposite hydrogels of 6 mm diameter and 400 μm thickness were prepared in a 96-well plates. Then, hMSCs were trypisinized and seeded onto the hydrogels at a density of 10 000 cells/hydrogel in normal growth media. After 24 and 48 h of cell seeding, the normal media were removed and the hydrogels were washed with PBS. The prepared Live/Dead assay reagent from Calcein AM and Ethidium Homodimer (Santa Cruz Biotechnology, Inc., USA) were added to the nanocomposites and incubated for 30 min at 37 °C. The samples were washed with PBS thrice, and imaged using the epifluorescence microscope (TE2000-S, Nikon, USA). Cell cycle analysis was performed using the BD Accuri C6 Flow Cytometer and propidium iodine (PI) stain following manufacture's protocol. Prior to seeding, hMSCs were starved for 24 h and then seeded on nanocomposite hydrogels. Cells seeded on each composition were trypsinized at two separate time points (24 and 72 h) and fixed in cold 70% ethanol. Cell pellets were formed and washed in PBS, followed by incubation in a PI staining solution at 37 °C for 30 min. Cells were stored at 4 °C until analysis. For 3D encapsulation, trypsinized MC3T3s were pelleted and subsequently resuspended within the nanocomposite prepolymer solution, which was maintained at 37 °C, and gels were formed on glass coverslips under previously described UV conditions. Coverslips with gels were stored in a 24-well plate with enough media to completely cover the gels for the required time points. Both live/dead

DOI: 10.1021/acsnano.5b03918
ACS Nano 2016, 10, 246−256

and actin cytoskeletal staining was performed according to manufacture's protocol.

Statistical Analysis. The experimental data were presented as mean and standard deviations (n = 5 or 6). GraphPad Prism 5 was used to perform statistical analysis using nonparametric tests and one-way analysis of variance (ANOVA). Tukey's posthoc analysis was used for pairwise comparisons and the statistical significance was defined as $*p < 0.05$, $**p < 0.01$, $***p < 0.005$.

ASSOCIATED CONTENT

Supporting Information

The Supporting Information is available free of charge on the ACS Publications website at DOI: 10.1021/acsnano.5b03918.

Physical and chemical characterizations; Stress and frequency sweeps of nanocomposites; *in vitro* cytocompatibility and encapsulation of hMSCs and preosteoblast within nanocomposite hydrogels (PDF)

AUTHOR INFORMATION

Corresponding Author

*E-mail: gaharwar@tamu.edu.

Author Contributions

M.K.J. and A.K.G. designed the experiments and wrote the manuscript. J.R.X. and P.D. contributed to materials synthesis and mechanical characterizations. J.K.C. contributed in the cell culture work and editing the manuscript. D.A. contributed to the rheology, the interpretation of chemical interactions with XPS data and manuscript preparation.

Notes

The authors declare no competing financial interest.

ACKNOWLEDGMENTS

We would like to acknowledge Ashish Thakur for his help with cell cycle analysis and Karthikeyan Baskaran for hydrogel preparation.

REFERENCES

(1) Hoffman, A. S. Hydrogels for Biomedical Applications. *Adv. Drug Delivery Rev.* **2012**, *64*, 18−23.

(2) Langer, R.; Tirrell, D. A. Designing Materials for Biology and Medicine. *Nature* **2004**, *428*, 487−492.

(3) Lutolf, M.; Hubbell, J. Synthetic Biomaterials as Instructive Extracellular Microenvironments for Morphogenesis in Tissue Engineering. *Nat. Biotechnol.* **2005**, *23*, 47−55.

(4) Burdick, J. A.; Murphy, W. L. Moving from Static to Dynamic Complexity in Hydrogel Design. *Nat. Commun.* **2012**, *3*, 1269.

(5) Kerativitayanan, P.; Carrow, J. K.; Gaharwar, A. K. Nanomaterials for Engineering Stem Cell Responses. *Adv. Healthcare Mater.* **2015**, *4*, 1600−1627.

(6) Gaharwar, A. K.; Peppas, N. A.; Khademhosseini, A. Nanocomposite Hydrogels for Biomedical Applications. *Biotechnol. Bioeng.* **2014**, *111*, 441−453.

(7) Seliktar, D. Designing Cell-Compatible Hydrogels for Biomedical Applications. *Science* **2012**, *336*, 1124−1128.

(8) Purcell, B. P.; Lobb, D.; Charati, M. B.; Dorsey, S. M.; Wade, R. J.; Zellars, K. N.; Doviak, H.; Pettaway, S.; Logdon, C. B.; Shuman, J. A. Injectable and Bioresponsive Hydrogels for On-demand Matrix Metalloproteinase Inhibition. *Nat. Mater.* **2014**, *13*, 653−661.

(9) Xia, L.-W.; Xie, R.; Ju, X.-J.; Wang, W.; Chen, Q.; Chu, L.-Y. *Nat. Commun.* **2013**, *4*, 2226.

(10) Gaharwar, A. K.; Arpanaei, A.; Andresen, T. L.; Dolatshahi-Pirouz, A. 3D Biomaterial Microarrays for Regenerative Medicine: Current State-of-the-Art, Emerging Directions and Future Trends. *Adv. Mater.* **2016**, DOI: 10.1002/adma.201503918.

(11) Gong, J. P.; Katsuyama, Y.; Kurokawa, T.; Osada, Y. Double-Network Hydrogels with Extremely High Mechanical Strength. *Adv. Mater.* **2003**, *15*, 1155−1158.

(12) Okumura, Y.; Ito, K. The Polyrotaxane Gel: A Topological Gel by Figure-of-Eight Cross-links. *Adv. Mater.* **2001**, *13*, 485−487.

(13) Huang, T.; Xu, H. G.; Jiao, K. X.; Zhu, L. P.; Brown, H. R.; Wang, H. L. A Novel Hydrogel with High Mechanical Strength: A Macromolecular Microsphere Composite Hydrogel. *Adv. Mater.* **2007**, *19*, 1622−1626.

(14) Wang, Q.; Mynar, J. L.; Yoshida, M.; Lee, E.; Lee, M.; Okuro, K.; Kinbara, K.; Aida, T. High-water-content Mouldable Hydrogels by Mixing Clay and a Dendritic Molecular Binder. *Nature* **2010**, *463*, 339−343.

(15) Haraguchi, K.; Takehisa, T. Nanocomposite Hydrogels: A Unique Organic−Inorganic Network Structure with Extraordinary Mechanical, Optical, and Swelling/De-swelling Properties. *Adv. Mater.* **2002**, *14*, 1120−1124.

(16) Carrow, J. K.; Gaharwar, A. K. Bioinspired Polymeric Nanocomposites for Regenerative Medicine. *Macromol. Chem. Phys.* **2015**, *216*, 248.

(17) Sun, J.-Y.; Zhao, X.; Illeperuma, W. R. K.; Chaudhuri, O.; Oh, K. H.; Mooney, D. J.; Vlassak, J. J.; Suo, Z. Highly Stretchable and Tough Hydrogels. *Nature* **2012**, *489*, 133−136.

(18) Nichol, J. W.; Koshy, S. T.; Bae, H.; Hwang, C. M.; Yamanlar, S.; Khademhosseini, A. Cell-laden Microengineered Gelatin Methacrylate Hydrogels. *Biomaterials* **2010**, *31*, 5536−5544.

(19) Shin, S. R.; Aghaei-Ghareh-Bolagh, B.; Dang, T. T.; Topkaya, S. N.; Gao, X.; Yang, S. Y.; Jung, S. M.; Oh, J. H.; Dokmeci, M. R.; Tang, X.; et al. Cell-laden Microengineered and Mechanically Tunable Hybrid Hydrogels of Gelatin and Graphene Oxide. *Adv. Mater.* **2013**, *25*, 6385−6391.

(20) Shin, S. R.; Jung, S. M.; Zalabany, M.; Kim, K.; Zorlutuna, P.; Kim, S. b.; Nikkhah, M.; Khabiry, M.; Azize, M.; Kong.; et al. A. Carbon-Nanotube-Embedded Hydrogel Sheets for Engineering Cardiac Constructs and Bioactuators. *ACS Nano* **2013**, *7*, 2369−2380.

(21) Shin, S. R.; Bae, H.; Cha, J. M.; Mun, J. Y.; Chen, Y.-C.; Tekin, H.; Shin, H.; Farshchi, S.; Dokmeci, M. R.; Tang, S.; et al. A. Carbon Nanotube Reinforced Hybrid Microgels as Scaffold Materials for Cell Encapsulation. *ACS Nano* **2012**, *6*, 362−372.

(22) Xavier, J. R.; Thakur, T.; Desai, P.; Jaiswal, M. K.; Sears, N.; Cosgriff-Hernandez, E.; Kaunas, R.; Gaharwar, A. K. Bioactive Nanoengineered Hydrogels for Bone Tissue Engineering: A Growth-Factor-Free Approach. *ACS Nano* **2015**, *9*, 3109−3118.

(23) Jana, N. R.; Chen, Y.; Peng, X. Size- and Shape-Controlled Magnetic (Cr, Mn, Fe, Co, Ni) Oxide Nanocrystals *via* a Simple and General Approach. *Chem. Mater.* **2004**, *16*, 3931−3935.

(24) Park, J.; An, K.; Hwang, Y.; Park, J.-G.; Noh, H.-J.; Kim, J.-Y.; Park, J.-H.; Hwang, N.-M.; Hyeon, T. Ultra-large-scale Syntheses of Monodisperse Nanocrystals. *Nat. Mater.* **2004**, *3*, 891−895.

(25) Jaiswal, M. K.; De, M.; Chou, S. S.; Vasavada, S.; Bleher, R.; Prasad, P. V.; Bahadur, D.; Dravid, V. P. Thermoresponsive Magnetic Hydrogels as Theranostic Nanoconstructs. *ACS Appl. Mater. Interfaces* **2014**, *6*, 6237−6247.

(26) Amstad, E.; Gillich, T.; Bilecka, I.; Textor, M.; Reimhult, E. Ultrastable Iron Oxide Nanoparticle Colloidal Suspensions Using Dispersants with Catechol-derived Anchor Groups. *Nano Lett.* **2009**, *9*, 4042−4048.

(27) Viola, K. L.; Sbarboro, J.; Sureka, R.; De, M.; Bicca, M. A.; Wang, J.; Vasavada, S.; Satpathy, S.; Wu, S.; Joshi, H.; et al. Towards Non-invasive Diagnostic Imaging of Early-stage Alzheimer's Disease. *Nat. Nanotechnol.* **2015**, *10*, 91−98.

(28) Xie, J.; Xu, C.; Kohler, N.; Hou, Y.; Sun, S. Controlled PEGylation of Monodisperse Fe_3O_4 Nanoparticles for Reduced Non-specific Uptake by Macrophage Cells. *Adv. Mater.* **2007**, *19*, 3163−3166.

(29) Damasceno, P. F.; Engel, M.; Glotzer, S. C. Predictive Self-assembly of Polyhedra into Complex Structures. *Science* **2012**, *337*, 453−457.

(30) Chimene, D.; Alge, D. L.; Gaharwar, A. K. Two-dimensional Nanomaterials for Biomedical Applications: Emerging Trends and Future Prospects. *Adv. Mater.* **2015**, *27*, 7261−7284.
(31) Bigi, A.; Cojazzi, G.; Panzavolta, S.; Roveri, N.; Rubini, K. Stabilization of Gelatin Films by Crosslinking with Genipin. *Biomaterials* **2002**, *23*, 4827−4832.
(32) Hutson, C. B.; Nichol, J. W.; Aubin, H.; Bae, H.; Yamanlar, S.; Al-Haque, S.; Koshy, S. T.; Khademhosseini, A. Synthesis and Characterization of Tunable Poly (ethylene glycol): Gelatin Methacrylate Composite Hydrogels. *Tissue Eng., Part A* **2011**, *17*, 1713−1723.
(33) Thakur, T.; Xavier, J. R.; Cross, L.; Jaiswal, M. K.; Mondragon, E.; Kaunas, R.; Gaharwar, A. K. Photocrosslinkable and Elastomeric Hydrogels for Bone Regeneration. *J. Biomed. Mater. Res., Part A* **2016**, DOI: 10.1002/jbm.a.35621.
(34) Rao, Y. Gelatin−clay Nanocomposites of Improved Properties. *Polymer* **2007**, *48*, 5369−5375.
(35) Shin, H.; Olsen, B. D.; Khademhosseini, A. Gellan gum microgel-reinforced cell-laden gelatin hydrogels. *J. Mater. Chem. B* **2014**, *2*, 2508−2516.
(36) Banerjee, A.; Arha, M.; Choudhary, S.; Ashton, R. S.; Bhatia, S. R.; Schaffer, D. V.; Kane, R. S. The Influence of Hydrogel Modulus on the Proliferation and Differentiation of Encapsulated Neural Stem Cells. *Biomaterials* **2009**, *30*, 4695−4699.
(37) Skardal, A.; Zhang, J.; McCoard, L.; Oottamasathien, S.; Prestwich, G. D. Dynamically Crosslinked Gold Nanoparticle−hyaluronan Hydrogels. *Adv. Mater.* **2010**, *22*, 4736−4740.
(38) Cha, C.; Shin, S. R.; Gao, X.; Annabi, N.; Dokmeci, M. R.; Tang, X. S.; Khademhosseini, A. Controlling Mechanical Properties of Cell-laden Hydrogels by Covalent Incorporation of Graphene Oxide. *Small* **2014**, *10*, 514−523.
(39) Wang, N.; Tytell, J. D.; Ingber, D. E. Mechanotransduction at a Distance: Mechanically Coupling the Extracellular Matrix with the Nucleus. *Nat. Rev. Mol. Cell Biol.* **2009**, *10*, 75−82.
(40) Ingber, D. E. Cellular Mechanotransduction: Putting all the Pieces Together Again. *FASEB J.* **2006**, *20*, 811−827.
(41) Murphy, W. L.; McDevitt, T. C.; Engler, A. J. Materials as Stem Cell Regulators. *Nat. Mater.* **2014**, *13*, 547−557.
(42) Wen, J. H.; Vincent, L. G.; Fuhrmann, A.; Choi, Y. S.; Hribar, K. C.; Taylor-Weiner, H.; Chen, S.; Engler, A. J. Interplay of Matrix Stiffness and Protein Tethering in Stem Cell Differentiation. *Nat. Mater.* **2014**, *13*, 979.
(43) Sun, S.; Zeng, H.; Robinson, D. B.; Raoux, S.; Rice, P. M.; Wang, S. X.; Li, G. Monodisperse MFe_2O_4 (M = Fe, Co, Mn) Nanoparticles. *J. Am. Chem. Soc.* **2004**, *126*, 273−279.

NOTE ADDED AFTER ASAP PUBLICATION

This paper published ASAP on 12/31/15. Figure 1(d) was corrected and the revised version was reposted on 1/14/16.

DOI: 10.1021/acsnano.5b03918
ACS Nano 2016, 10, 246−256